Structure of neutral aluminum clusters Al_n ($2 \leqslant n \leqslant 23$): Genetic algorithm tight-binding calculations

Feng-Chuan Chuang,* C. Z. Wang, and K. H. Ho
Ames Laboratory-U.S. Department of Energy and Department of Physics and Astronomy, Iowa State University, Ames, Iowa 50011, USA
(Received 23 January 2006; published 27 March 2006)

We performed global structural optimizations for neutral aluminum clusters Al_n (n up to 23) using a genetic algorithm (GA) coupled with a tight-binding interatomic potential. Structural candidates obtained from our GA search were further optimized by using first-principles total energy calculations. We report the lowest energy structures of neutral Al_n ($n=2-23$). We found that the icosahedral structure of Al_{13} serves as the core for the growth of aluminum clusters from Al_{14} to Al_{18}.

DOI: 10.1103/PhysRevB.73.125431 PACS number(s): 36.40.Mr, 36.40.Qv

I. INTRODUCTION

An enormous effort has been invested in understanding the size-dependent structural and physical properties of aluminum clusters.[1–12] It is well accepted that for Al_n ($n \leqslant 5$) the ground-state structures are planar, while for Al_n ($6 \leqslant n \leqslant 11$) the lowest energy structures are all based on the octahedron of Al_6 which serves as the nucleation center for the growth of these clusters. For medium-sized neutral Al_n ($12 \leqslant n \leqslant 23$) clusters, recent study by Akola *et al.*[11] showed that the isomers derived from the Al_{13} icosahedral structure are energetically more favorable compared to those from the decahedral or octahedral structures. Akola *et al.*[12] also studied anionic aluminum clusters and showed that the neutral and anionic clusters share the common lowest energy structures in sizes ranging from 12 to 15. In addition, for larger anionic clusters, Al_{19}^-, Al_{20}^- andAl_{23}^-, the ground-state structures proposed by Akola *et al.* produce photoelectron spectra in very good agreement with experimental data.[12] To the best of our knowledge, there are no detailed studies on the ground-state structures of Al_{16}, Al_{17}, Al_{18}, Al_{21}, and Al_{22} using first-principles calculations.

In this paper, an unbiased global search for the ground-state structures of aluminum clusters with sizes ranging from $n=6$ to $n=23$ atoms was performed using a genetic algorithm (GA) coupled with a tight-binding (TB) interatomic potential. Low energy candidates obtained from the GA/TB search are further optimized using first-principles total energy calculations. We note that two recent studies[13–15] have also used a genetic algorithm coupled with classical potentials to search for the lowest energy structures of the aluminum clusters. It has been shown that the lowest energy structures under a specific potential model could be obtained using a genetic algorithm. Nevertheless, the classical potentials usually fail to reproduce the correct energy ordering of the isomers compared to first-principles calculations. Therefore, it would be interesting to adopt a more accurate interatomic potential such as tight-binding potential to the genetic algorithm for a global optimization. By combining the GA/TB search with first-principles calculations, we have successfully determined the lowest energy structures for Al_n ($n=6$ to 23). Moreover, we observed a clear growth pattern of Al_n ($n=3$ to 23).

This paper is arranged as follows: In Sec. II, we discuss briefly our computational methods. Our results and discussions are presented in Sec. III. Finally, a conclusion is drawn in Sec. IV.

II. COMPUTATIONAL METHODS

Genetic algorithm (GA) has been successfully used in global structural optimizations for C_{60} (Ref. 16) and medium-sized silicon clusters.[17] Recently, we have successfully applied the genetic algorithm to search for the reconstructions of high index silicon surfaces,[18,19] as well as the atomic structures of Si magic clusters on Si(111) 7×7 surface.[20]

In the present study, three types of operations, i.e., mating, mirror, and rotation, have been used to generate structures in genetic algorithm optimization. In the mating operation both parents A and B are randomly rotated about their centers of mass which are set to be the origin. Then, by simply cutting the parents' structures through the plane of $z=0$ and permuting the lower halves (atoms below the plane of $z=0$) of the parent structures A and B, two new offspring structures C and D can be created. If the number of atoms in the offspring structure does not match with that in the parent, parents A and B are shifted along the z axis in order to achieve the correct match. In the present study, two structures from the population pool are picked as parents and a child structure is generated by mating the lower half of parent A with the upper half of parent B. In the mirror operation, a parent structure is picked from the population pool and rotated randomly about its center of mass, which is set to be the origin. This parent is shifted along the z axis in order to balance the number of atoms in both halves. An offspring is created simply by duplicating the lower half into the upper half. The new upper half is shifted along the z axis to reach a appropriate distance between two halves. Finally in the third operation, *rotation*, a parent structure is picked from the population pool and rotated randomly about its center of mass, which is set tobe the origin. A child structure is created by rotating the upper half in a random angle, while the bottom half is held.

In order to maintain the diversity in the population pool, it is very important to have a structural comparison algorithm

when updating the population pool. Before describing the procedures of the structural comparison algorithm, we will first define the translation-rotation (T-R) operation below.

The translation-rotation operation rotates the cluster to a certain orientation defined by any three chosen atoms in a cluster. First, a translation is performed to make the first chosen atom as origin. Next, a rotation on the cluster is performed to make the line connecting the first and second atoms oriented along the z axis. Finally, another rotation is performed to make third atom lie on the x-z plane.

Having described the T-R operation, we now elaborate on the algorithm to compare two clusters A and B with the same size of N atoms. We first picked three atoms in cluster A and perform the T-R operation to set its orientation. Then a total number of $N(N-1)(N-2)$ sets of three-atoms in cluster B can be selected. If cluster B is the same as cluster A, then there should be a particular set of three-atom coordinates in B identical to the chosen three-atom coordinates in A after the T-R operation. Therefore, for each set of three-atom coordinates in cluster B, we performed the T-R operation and calculate the coordinates deviations of these atoms from those of the corresponding atoms in cluster A. If the maximum deviation is less than 0.35 Å, then the two structures are regarded as identical. A similar algorithm to perform the structural comparison between two clusters can also be found in Ref. 21.

The genetic algorithm optimizations in the present study are proceeded as follows: In generation zero, a population pool of $p=30$ structures for a given cluster size n are generated by putting n atoms randomly in a simulation cubic box with a appropriate length. The structures are relaxed to their local minima using a tight-binding potential with the steepest descent method. In each subsequent generation, three types of operations (i.e., mating, mirror, and rotation as described above) are used to generate 15 new structures: 12 from mating, one from the mirror, and two from the rotation operations. Then, the 15 new structures are relaxed to their local minima by tight-binding calculations. The population pool is updated if the newly relaxed structures are not identical to any isomer inside the population pool and have lower energies. The genetic algorithm optimizations were proceeded up to 800 generations.

At the end of the global minimum structure search, as many as $p=30$ structures remain as possible candidates. The selected candidates are further optimized using first-principles total energy calculations. Our first-principles calculations were done using Vienna *Ab initio* Simulation Package (VASP), which is based on density functional theory (DFT), and uses ultrasoft pseudopotentials and plane waves basis.[22] Local density approximation is used for the exchange-correlation functional, and spin polarized calculations are also performed. The kinetic energy cutoff is set to be 170 eV. The structural optimization is done with the conjugate gradient algorithm and without symmetry until the forces on the atoms are less than 0.001 eV/Å. For clusters containing fewer than 15 atoms, the length of supercell is set to be 15 Å. For Al_{15}, Al_{16}, Al_{17}, Al_{18}, and Al_{19} to Al_{23}, the lengths of supercell are 16, 17, 17, 18, and 19 Å, respectively.

We note that the candidate structures from the GA/TB search undergo substantial relaxations upon first-principles optimizations. Sometimes several candidate structures can be relaxed into the same final structure after the first-principle optimizations.[22] Therefore the energy differences and energy ordering of the isomers from the GA/TB calculations are not the same as the first-principles results. However, we found that for cluster size less than 13, we can always locate the known ground-state structure by choosing the lowest ten structures from the GA pool as the initial structures for first-principles optimizations. In order to ensure that the ground-state structures for large clusters are not missed, we have chosen, for each size of cluster, all the 30 candidate structures in the final GA pool as the initial structures for our first-principles optimizations.

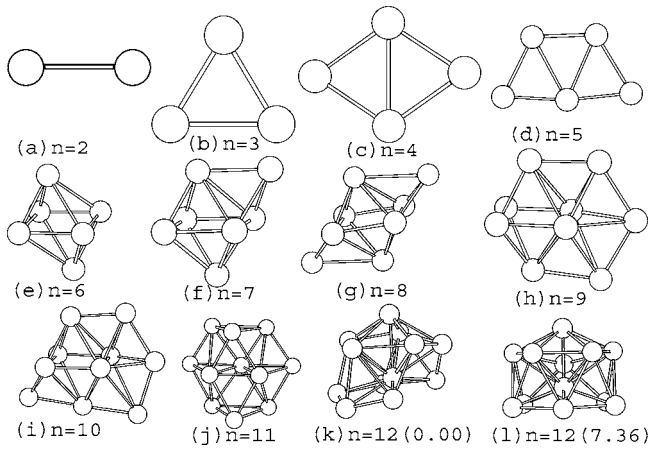

FIG. 1. (a) to (k) The lowest energy isomers of neutral Al_2 to Al_{12}. (l) is the lowest energy isomer of Al_{12}^-. The numbers in the parentheses and under the structures are relative energies per atom (in meV/atom) with respect to that of the lowest energy isomer of the same size.

III. RESULTS AND DISCUSSIONS

A. Small neutral Al_n clusters ($2 \leq n \leq 12$)

We performed structural optimizations using the genetic algorithm for aluminum clusters Al_6 to Al_{23}. The energies presented in this paper are all done using first-principles calculations. The lowest energy isomers for Al_2 to Al_{12} are shown in Fig. 1. For small clusters containing up to five atoms, the structural characteristic of the lowest energy isomers are planar, which is in agreement with several other first-principles studies.[6,5,8,9]

For clusters containing six to ten atoms, the geometries transform into a three-dimensional motif and the growth pattern is based on the octahedron of Al_6. The most stable isomer for Al_9 has the structural characteristics of Al_6 with three capped atoms on one side of the octahedron as shown in Fig. 1(h). The lowest energy isomer for Al_{10} is obtained by capping one more atom onto Al_9.

For Al_{11} and Al_{12}, the structures start to form motifs similar to an icosahedron of Al_{13}. For Al_{11}, our result is similar to the anionic cluster Al_{11}^- identified in the study of Rao and Jena.[8] For Al_{12}, we found that the two low energy structures are very close to those obtained by removing one atom from

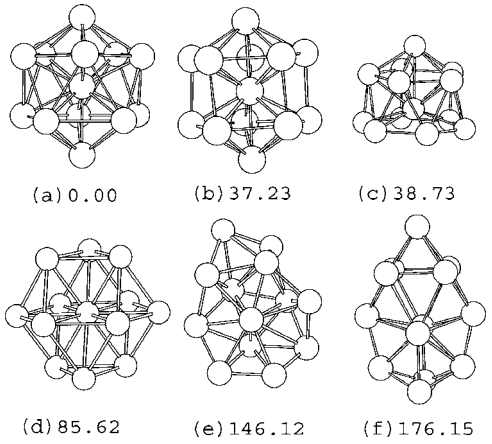

FIG. 2. Low energy isomers of Al_{13}. The numbers under the structures are the relative total energies per atom (in meV/atom) with respect to that of the lowest energy isomer.

an ideal icosahedron of Al_{13} as shown in Figs. 1(k) and 1(l). The lowest energy isomer shown in Fig. 1(k) has larger distortion than the one shown in Fig. 1(l). The energy difference per atom between the two isomers is 7.36 meV/atom. However, both isomers have the icosahedral origin of Al_{13} shown in Fig. 2(a).[2,6,11,7,9,5,8,12]

Our results for small clusters are consistent with the studies of Jones[5] and Rao and Jena.[8] for sizes ranging from two to ten. For Al_{11} and Al_{12}, the structures obtained from our study are nearly identical to those proposed by Rao and Jena.[8] The small differences in Al_{11} and Al_{12} between our results and previous results may be attributed to different pseudopotentials and exchange-correlation energy functional used in the studies.

B. Medium-size neutral Al_n clusters ($13 \leqslant n \leqslant 23$)

The six low energy isomers of Al_{13} are shown in Fig. 2. The lowest energy isomer is the icosahedron shown in Fig. 2(a). The energetic ranking of the three isomers shown in Figs. 2(a), 2(b), and 2(d) is in agreement with that of Akola *et al.*[11] We found that a new isomer named distorted icosahedron shown in Fig. 2(c) is the third lowest energy isomer. As we will see later, this isomer becomes another important

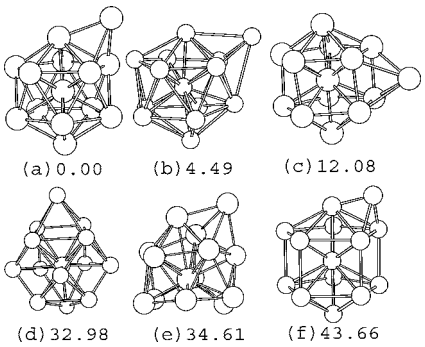

FIG. 3. Low energy isomers of Al_{14}. The numbers under the structures are relative energies per atom (in meV/atom) with respect to that of the lowest energy isomer.

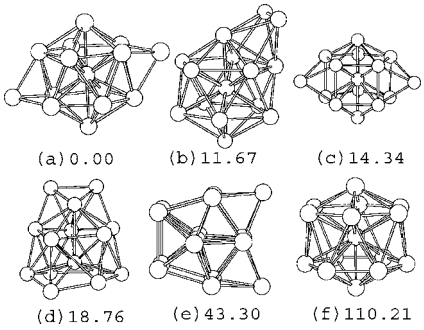

FIG. 4. Low energy isomers of Al_{15}. The numbers under the structures are relative energies per atom (in meV/atom) with respect to that of the lowest energy isomer.

building block beside the icosahedral isomer as the cluster increases in size. We denote this distorted icosahedron isomer as "1516" according to the number of stacking atoms in each layer. Following this notation we denote the icosahedron as "15151."

For Al_{14}, the low energy isomers contain either one of the building blocks from Al_{13}. Some isomers of Al_{14} can be obtained by capping one atom on the icosahedron of Al_{13} as shown in Figs. 3(a) and 3(b). The difference between Figs. 3(a) and 3(b) is the position of capped atoms. The lowest energy isomer is a capped icosahedron on one of its faces, whereas the second lowest energy isomer is a capped atom on one of the bonds of the icosahedron as shown in Fig. 3(b). Other low energy isomers shown in Figs. 3(c) and 3(f) are found to be one capped atom on the decahedron. Structures with one capped atom on a distorted icosahedron (denoted "1516") at different positions as shown in Figs. 3(d) and 3(e) are energetically not favorable.

For Al_{15}, five low energy isomers also contain the two distinct bases of Al_{13}. The lowest energy isomer is the symmetric bicapped icosahedron, which is in agreement with the study of Akola *et al.*[11] The other isomers can be named as the adjacent bicapped icosahedron shown in Fig. 4(b), the nonadjacent bicapped decahedron shown in Fig. 4(c), the adjacent bicapped distorted icosahedron, shown in Fig. 4(d), and the adjacent bicapped decahedron shown in Fig. 4(e). Other than capping, the atoms can also be embedded into the structure. A stacking layer of 16161 shown in Fig. 4(f) is obtained

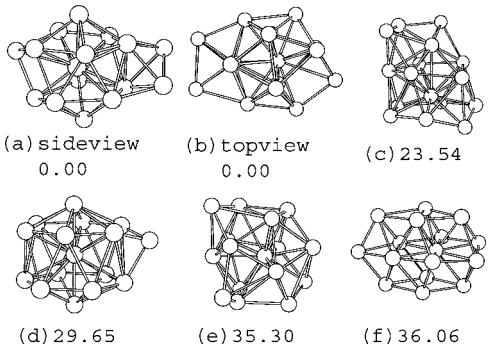

FIG. 5. Low energy isomers of Al_{16}. The numbers under the structures are relative energies per atom (in meV/atom) with respect to that of the lowest energy isomer.

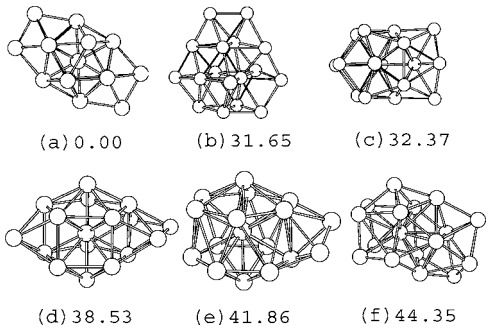

FIG. 6. Low energy isomers of Al_{17}. The numbers under the structures are relative energies per atom (in meV/atom) with respect to that of the lowest energy isomer.

by embedding two atoms into the outer surface of the icosahedral Al_{13}. From Al_{12} to Al_{15}, the growth motif starts to appear.

For Al_{16}, the low energy isomers grow in the same manner as Al_{14} and Al_{15} did. Low energy isomers are obtained by capping three more atoms to the surface of Al_{13} isomers in different ways. The lowest energy isomer for Al_{16} is obtained by capping one more atom to the bicapped icosahedron Al_{15}, resulting in two adjacent capped atoms and an individually capped atom as shown in Figs. 5(a) and 5(b). It shows that the individually capped atom is partially embedded into the icosahedral surface. Other isomers along with their relative energies to the lowest energy structure are also shown in Fig. 5 for comparison.

For Al_{17}, the lowest energy structure consists of four capped atoms on an icosahedron, with two sets of two adjacent atoms capping on opposite symmetric positions as shown in Fig. 6(a). This is a different structure and has not been reported in the literature. The other isomers of Al_{17} are also shown in Fig. 6 in order to have a clear comparison.

For Al_{18}, the lowest energy structure shown in Fig. 7(a) is formed by capping one more atom to the lowest energy isomer of Al_{17}, shown in Fig. 6(a). The isomer proposed by Ahlrichs and Elliott[7] as shown in Fig. 6(g) is obtained by removing five corner atoms from the decahedron of Al_{23}, shown in Fig. 9(f). Note that motifs derived from the icosahedron of Al_{13} have better energies than those derived from the decahedron of Al_{13}. In this regard, the icosahedron is the preferred nucleation center for Al_{14} to Al_{18}.

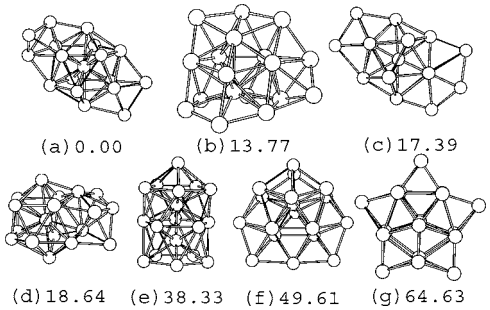

FIG. 7. Low energy isomers of Al_{18}. The numbers under the structures are relative energies per atom (in meV/atom) with respect to that of the lowest energy isomer.

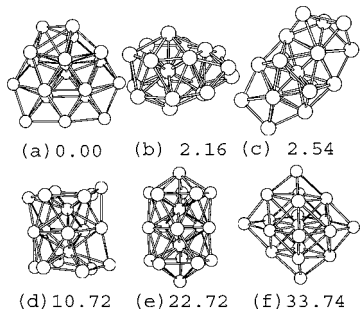

FIG. 8. Low energy isomers of Al_{19}. The numbers under the structures are relative energies per atom (in meV/atom) with respect to that of the lowest energy isomer.

For Al_{19}, the lowest energy isomer is the one with five adjacent atoms and a individually atom capping on the decahedron as shown in Fig. 8(a), which is the second lowest anionic isomer in the study of Akola *et al.* in Ref. 12. Other low energy isomers (bicaped 16161, bicapped Al_{17}, and 61516) are shown in Figs. 8(b)–8(d). Two most well-known isomers of Al_{19}, the double icosahedron (1515151) and the octahedron, are shown in Figs. 8(e) and 8(f). The double icosahedron could also be classified as six adjacent capped atoms on one side of an icosahedron and this double icosahedron structure is not the lowest energy structure according to first-principles calculations. The other well-known geometrically magic isomer is the octahedron as shown in Fig. 8(d). We found that numerous isomers have energies lower than the well-known double icosahedron shown in Fig. 8(e). Here, we can clearly see that the geometrically magic cluster is not always necessarily the energetically favorable motif.

For Al_{20}, the lowest energy structure shown in Fig. 9(a) has one atom embedded into the double icosahedron of Al_{19}. The structure (denoted "1515161") is prolate and its internal structure is a hybrid between an icosahedral stacking and hexagonal pyramid. This structure shown is also the lowest energy anionic isomer of Al_{20}^- in Ref. 12. The second lowest energy isomer is 161516 shown in Fig. 9(b). The six-capped 15161 and five-capped 16161 are shown in Figs. 9(c) and 9(d), respectively. The capped icosahedron and capped octahedron are shown in Figs. 9(e) and 9(f).

For Al_{21}, the lowest energy structure from our calculations is shown in Fig. 10(a). This structure is obtained by capping one atom onto the side of the lowest energy isomer

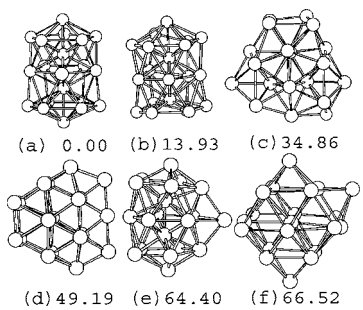

FIG. 9. Low energy isomers of Al_{20}. The numbers under the structures are relative energies per atom (in meV/atom) with respect to that of the lowest energy isomer.

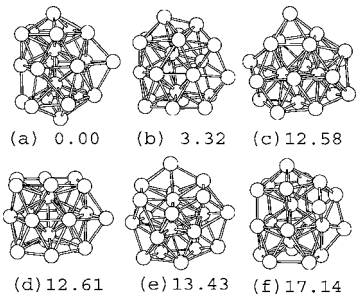

FIG. 10. Low energy isomers of Al_{21}. The numbers under the structures are relative energies per atom (in meV/atom) with respect to that of the lowest energy isomer.

of Al_{20}, shown in Fig. 9(a). Several low energy isomers are also shown in Fig. 10. It is interesting to note that the isomer shown in Fig. 10(b) is a precursor of Al_{22} [Fig. 11(c)], and Fig. 10(c) is the precursor for Al_{22} [Fig. 11(b)] and Al_{23} [Fig. 11(d)].

The low energy structures of Al_{22} and Al_{23} are shown in Fig. 11. For Al_{22}, the first two low energy isomers as shown in Figs. 11(a) and 11(b) are close in energies. A noteworthy feature is that by adding one more atom on second lowest energy isomer of Al_{22} in Fig. 9(b), we obtain the lowest energy isomer of Al_{23} shown in Fig. 11(d). This lowest energy isomer of Al_{23} is also the lowest energy anionic cluster in Ref. 12. In fact, we found several structures that have energies lower than that of the icosahedron and decahedron as shown in Figs. 11(f) and 11(g), respectively. One of those low energy isomers is shown in Fig. 11(e).

Among the lowest energy structures for Al_{13} to Al_{23} obtained from our present study, the structures of Al_{16}, Al_{17}, Al_{18}, Al_{21}, and Al_{22} had been previously unknown, while the structures for Al_{13} to Al_{15}, Al_{19}, Al_{20} and Al_{23} are in agreement with those reported in the literature.[12] We also show that the geometrically magic isomers of Al_{19} and Al_{23} are not necessarily the energetically favorable ones.

C. Relative stabilities

The binding energies (per atom) as a function of cluster size are plotted in Fig. 12(a). The binding energy curve can

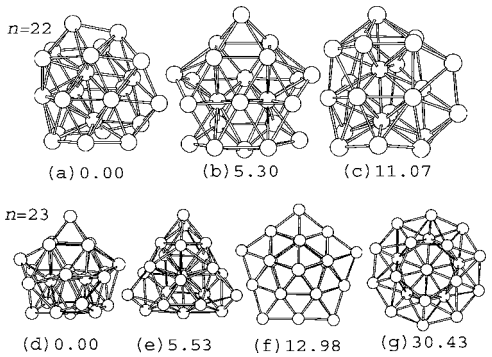

FIG. 11. (a), (b), and (c) are isomers of Al_{22}, whereas (d), (e), (f), and (g) are that of Al_{23}. The numbers under the structures are relative energies per atom (in meV/atom) with respect to that of the lowest energy isomer of the same size.

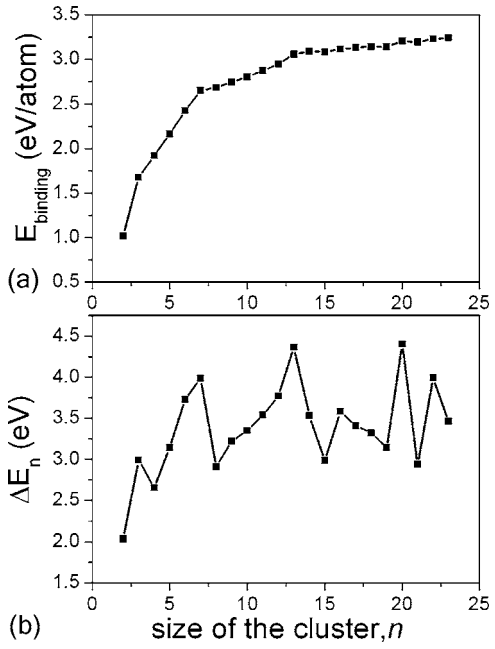

FIG. 12. (a) The binding energy vs size of the cluster. (b) The fragmentation energy ($\Delta E_{n,1}=E_1+E_{n-1}-E_n$) vs size of the cluster. The most dominant channel of the fragmentation energy is the evaporation of an atom from the cluster.

be roughly divided into three regions: $n<7$ where the binding energy increases rapidly as the cluster size increases, $7<n<13$ where the binding energy increases moderately with size, and $n>13$ where binding energy increases slowly. There is also a small energy jump for $n>20$. There seems a delayed correlation between the binding energy and changes in the structure growth pattern. For n from 2 to 5, the structures are planar. For n from 6 to 10, the structures become three dimensional with additional capped atoms on the octahedron of Al_6. However, the binding energy changes slope at $n=7$. For n from 11 to 13, the clusters start to form the icosahedral-like motif but the binding energy curve does not change its slope until $n=13$. The growth pattern from Al_{14} to Al_{18} is mainly based on the mechanism of capping extra atoms on the icosahedron of Al_{13}. For $n\geqslant 19$, the structures undergo additional structural transformation. The lowest energy isomer of Al_{19}consists of five adjacent atoms and a individually atom capping on the decahedron isomer of Al_{13} as shown in Fig. 8(a). However, the small energy kink in the binding energy curve does not occur at $n=19$ but at $n=20$. Al_{20} and Al_{21} share the same motif of capping atoms on the double icosahedron. For $n=22$ and 23, the aluminum clusters begin to grow into a different motif.

Studies of fragmentation pathways and dissociation energies provide useful information for understanding the stability of the clusters. It has been found that clusters which frequently appear in the fragmentation products are likely to be relatively stable clusters. The energy, $\Delta E_{n,m}$, needed to dissociate a neutral n-atom cluster into m-atom and $(n-m)$-atom clusters is given by

$$\Delta E_{n,m} = E_m + E_{n-m} - E_n, \tag{1}$$

where E_m, E_{n-m}, and E_n are the total energies of the clusters with m, $n-m$, and n atoms, respectively. We found that for

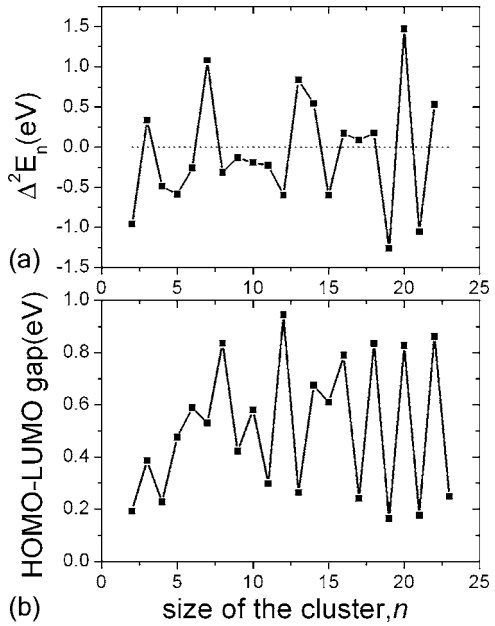

FIG. 13. (a) The second difference in energy and (b) the HOMO-LUMO gap as a function of the number of atoms in clusters.

the fragmentation of the neutral clusters, the most dominant channel is the evaporation of an atom from the cluster. This result is in agreement with the study of Al_n (n up to 15) by Rao and Jena.[8] The fragmentation energies for the energetically most favorable channels obtained from Eq. (1) are plotted in Fig. 12(b). Clusters with a larger fragmentation energies should be more stable. As one can see from the plot of Fig. 12(b), the relative stable isomers from our present study are found to be $n=3$, 7, 13, 16, 20, and 22.

The relative stability of the clusters can also be classified through second difference in energy defined as

$$\Delta^2 E_n = -2 \times E_n + E_{n+1} + E_{n-1}. \quad (2)$$

$\Delta^2 E_n$ as a function of cluster size is plotted in Fig. 13(a). The stability analysis based on this plot also shows that the relative stable isomers are $n=3$, 7, 13, 20, and 22, in agreement with the fragmentation analysis. Note that $n=16$ shows only marginal stability.

We also study the HOMO-LUMO (highest occupied molecular orbital-lowest unoccupied molecular orbital) gaps of the Al clusters. The HOMO-LUMO gaps of the lowest-energy isomers of each cluster size are evaluated using spin-polarization DFT calculations. The results as plotted in Fig. 13(b) show that the clusters with even number of atom tend to have relative larger gaps than two adjacent clusters with odd number atoms except for $n<6$ where spin effects are important. We do not find a strong correlation between the HOMO-LUMO gaps and the energetic stability of the cluster except for Al_{20} where both fragmentation energy and HOMO-LUMO gaps are large.

Finally, we note that the energy differences between first and second lowest energy isomers are large for clusters of sizes $n=13$ (37.23 meV/atom), 16 (23.54 meV/atom), and 17 (31.65 meV/atom). For Al_{13} and Al_{17}, this large energy difference may be attributed to the fact that the first isomer has much higher symmetry than that of the second isomer. For Al_{16}, the first and second isomers are based on different motifs: the first isomer is formed by capping three atoms onto the icosahedral (15151) Al_{13}, while the second isomer is based on the distorted icosahedral (1516) Al_{13}. On the other hand, the energy differences between first and second lowest energy isomers in other clusters are small (less than 14 meV/atom), suggesting that at finite temperature, multi-isomers of the same size may coexist.

IV. CONCLUSION

We have performed global structural optimizations for aluminum neutral clusters Al_n, n up to 23 atoms. The low energy isomers of Al_2-Al_{23} are obtained based on first-principles calculations. Lowest-energy structures for Al_{16}, Al_{17}, Al_{18}, Al_{21}, and Al_{22} have been determined from our calculations. From analysis of energetics, the sizes of the relative stable clusters are found to be $n=7$, 13, 20, and 22.

We have also studied the growth motif for Al_n ($2 \leqslant n \leqslant 23$). For n from 2 to 5, the structures are planar. For n from six to ten, the structures become three dimensional with additional capped atoms on the octahedron of Al_6. For n from 11 to 13, the clusters start to form the icosahedral-like motif. The growth pattern from Al_{14} to Al_{18} is mainly based on the mechanism of capping extra atoms on the icosahedron of Al_{13}. For $n \geqslant 19$, the structures undergo additional structural transformations. The lowest energy isomer of Al_{19} consists of five adjacent atoms and a individually atom capping on the decahedron isomer of Al_{13} as shown in Fig. 8(a). Al_{20} and Al_{21} share the same motif of capping atoms on the double icosahedron. For $n \geqslant 22$, the aluminum clusters begin to grow into a different motif.

ACKNOWLEDGMENTS

Ames Laboratory is operated for the U.S. Department of Energy by Iowa State University under Contract No. W-7405-Eng-82. This work was supported by the Director of Energy Research, Office of Basic Energy Sciences, including a grant of computer time at the National Energy Research Supercomputing Center (NERSC) in Berkeley and the EMSL computational resources at the Pacific Northwest National Laboratory.

*Corresponding author. Present address: Department of Physics, National Sun Yat-Sen University, Kaohsiung 804, Taiwan.

[1] T. H. Upton, Phys. Rev. Lett. **56**, 2168 (1986).
[2] Lars G. M. Pettersson, Charles W. Bauschlicher, Jr., and Timur Halicioglu, J. Chem. Phys. **87** 2205 (1987); Charles W. Bauschlicher, Jr. and Lars G. M. Pettersson, *ibid.* **87**, 2198 (1987).
[3] J. Y. Yi, D. J. Oh, J. Bernholc, and R. Car, Chem. Phys. Lett. **174**, 461 (1990); J. Y. Yi, Dirk J. Oh, and J. Bernholc, Phys. Rev. Lett. **67**, 1594 (1991).
[4] H.-P. Cheng, R. S. Berry, and R. L. Whetten, Phys. Rev. B **43**, 10647 (1991).
[5] R. O. Jones, Phys. Rev. Lett. **67**, 224 (1991); R. O. Jones, J. Chem. Phys. **99**, 1194 (1993).
[6] S. H. Yang, D. A. Drabold, J. B. Adams, and A. Sachdev, Phys. Rev. B **47**, 1567 (1993).
[7] Reinhart Ahlrichs and Simon D. Elliott, Phys. Chem. Chem. Phys. **1**, 13 (1999).
[8] B. K. Rao and P. Jena, J. Chem. Phys. **111**, 1890 (1999).
[9] H. Kawamura, V. Kumar, Q. Sun, and Y. Kawazoe, Phys. Rev. B **65**, 045406 (2001).
[10] M. D. Deshpande, D. G. Kanhere, Igor Vasiliev, and Richard M. Martin, Phys. Rev. B **68**, 035428 (2003).
[11] J. Akola, H. Hakkinen, and M. Manninen, Phys. Rev. B **58**, 3601 (1998).
[12] J. Akola, M. Manninen, H. Häkkinen, U. Landman, X. Li, and L.-S. Wang, Phys. Rev. B **60**, R11297 (1999); J. Akola, M. Manninen, H. Häkkinen, U. Landman, X. Li, and L.-S. Wang, *ibid.* **62**, 13216 (2000).
[13] Lesley D. Lloyd and Roy. L. Johnson, Chem. Phys. **236**, 107 (1998).
[14] Lesley D. Lloyd, Roy L. Johnston, Christopher Roberts, and Thomas V. Mortimer-Jones, ChemPhysChem **3**, 408 (2002).
[15] Jan-Ole Joswig and Michael Springborg, Phys. Rev. B **68**, 085408 (2003).
[16] D. M. Deaven and K. M. Ho, Phys. Rev. Lett. **75**, 288 (1995).
[17] K. M. Ho, A. A. Shvartsburg, B. C. Pan, Z. Y. Lu, C. Z. Wang, J. Wacker, J. L. Fye, and M. F. Jarrold, Nature **392**, 582 (1998).
[18] F. C. Chuang, C. V. Ciobanu, V. B. Shenoy, C. Z. Wang, and K. M. Ho, Surf. Sci. **573**, L375 (2004).
[19] F. C. Chuang, C. V. Ciobanu, C. Predescu, C. Z. Wang, and K. M. Ho, Surf. Sci. **578**, 183 (2005); F. C. Chuang, C. V. Ciobanu, C. Z. Wang, and K. M. Ho, J. Appl. Phys. **98**, 073507 (2005).
[20] F. C. Chuang, B. Liu, C. Z. Wang, T. L. Chan, and K. M. Ho, Surf. Sci. Lett. **598**, L339 (2005).
[21] E. Curotto, Alexander Matro, David L. Freeman, and J. D. Doll, J. Chem. Phys. **108**, 729 (1998).
[22] G. Kresse and J. Hafner, Phys. Rev. B **47**, R558 (1993); G. Kresse and J. Furthmuller, *ibid.* **54**, 11169 (1996).